Highly efficient capacitive deionization electrodes from electro spun carbon nanofiber membrane containing reduced graphene oxide and carbon nanotubes

Guoming Luo[a], Lixin Gao[a], Daquan Zhang[a,*], Jianli Zhang[b], Tong Lin[c]

[a]*Shanghai Key Laboratory of Materials Protection and Advanced Materials in Electric Power, School of Environment and Chemical Engineering, Shanghai University of Electric Power, Shanghai 200090, China, email: zhangdaquan@shiep.edu.cn (D. Zhang)*
[b]*Shenhua Guohua (Beijing) Electric Power Research Institute Co., Ltd, Beijing 100025, China*
[c]*Institute for Frontier Materials, Deakin University, Geelong, VIC 3216, Australia*

ABSTRACT

Carbon nanofibers containing reduced graphene oxide (RG) and carbon nanotubes (CNTs) were prepared via electro spinning and carbonization. The addition of carbon nanotubes was found to be embedded within the inner fibers and graphene sheets, which are beneficial to provide more defects and mesopores. Without any binder, the tri-component nanofibers were directly used as CDI electrodes, which showed a desalination capacity of 13.6 mg g^{-1} in a 500 mg L^{-1} NaCl solution with a remarkable cyclic stability and 98% capacitance retention after 1000 cycles of charging-discharging. The presence of reduced graphene oxide and carbon nanotubes was found to effectively improve conductivity and electro sorption efficiency. Such a tri-component carbon nanofibrous sheet may be useful for making high performance electrodes for various CDI applications.

Keywords: Carbon nanofibers; Electro spinning; Graphene; Capacitive deionization; Carbon nanotubes

1. Introduction

The shortage of drinking water has been a global issue due to environment contamination and population. In recent years, many technologies have been used to solve this problem, including multistage flash, electro-dialysis, ion exchange and reverse osmosis technologies [1–5]. The conventional desalination techniques, however, are often confined with excessive energy consumption, secondary pollution, low environmental friendliness and maintenance difficulty [3,6,7]. Recently, capacitive deionization (CDI) has emerged as a renewable, cost-effective desalination technology, drawing more and more attention in both industrial and scientific sectors [4].

CDI is based on a circulated capacitor where the positive and negative ions under an external direct voltage (usually below 2.0 V) can be attracted within the electrical double layer (EDL) formed between the charged electrodes and the salt solution. Similar to EDL capacitor, CDI is also required the electrodes being porous with large surface area and the desalination performance is strongly dependent on the electro sorption ability and kinetics [8]. In addition, energy storage electrode materials may very well be the source of leading, next-generation water treatment systems [5]. Various carbon materials such as activated carbon [10], carbon aerogels [11,12], carbon nanofibers (CNFs) [13], carbon nanotubes (CNTs) [14,15], and graphene [16,17] have been tested as super capacitor and CDI electrode materials. However, a polymeric binder has to be used for most electrode fabrication. Since the addition of binder reduces surface area and blocks pores, binder-free and self-sustainable electrode materials for CDI are highly desirable.

Recently, a few research groups reported the preparation of binder-free CDI carbon electrodes [18–21]. Yang et al. [21] reported a sponge-templated graphene electrode for potential applications in CDI. This binder-free carbon electrode showed an electro sorptive capacity of 4.95 mg g^{-1}. Xu

*Corresponding author.

et al. [20] prepared a nitrogen-doped 3D graphene sponge with an electro sorptive capacity of 21.0 mg g^{-1} in 500 mg L^{-1} NaCl solution.

Electro spinning is a simple but efficient technique to prepare nanofibers [22–24]. Binder-free carbon nanofiber sheets can be prepared by carbonization of electro spun nanofiber mats. The electro spun carbon nanofibers can be modified by adding the corresponding precursors into the electro spinning solution. Liuet al. [25] prepared porous carbon nanofibers by electro spinning polyacrylonitrile (PAN) solution containing dimethyl sulfone (DMSO$_2$) and subsequent carbonization. The carbon nanofiber sheets showed 4.5 times higher CDI electrical adsorption than the CNFs prepared by the PAN solution without DMSO$_2$. In general, the enhanced desalination capacities were attributed to the special nanostructure and double-layer properties of electrode materials [9]. In our previous work, a unique Cross-linked network structure consisting of one dimensional (i.e. nanofibers) and two-dimensional (i.e. graphene) carbon nanomaterials was found to contribute much to ion removal capacity [23]. It was reported that when carbon nanotubes or graphene were incorporated into electro spun carbon nanofibers in a similar manner, the presence of these carbon nanomaterials considerably improved the electric conductivity, mechanical properties of the electro spun carbon nanofibers. However, carbon nanofibers (CNFs) containing RG or carbon nanotubes (CNTs) have been little reported for CDI application. Qiu et al. [13] reported that carbon composite from reduced graphene oxide (RGO) and electro spun carbon nanofibers showed an electro sorption capacity of 7.2 mg g^{-1} in 400 mg L^{-1} NaCl aqueous solution.

Herein, we report the preparation of carbon nanofibers containing reduced graphene oxide and carbon nanotubes by electro spinning, followed by thermal treatment. The addition of carbon nanotubes was found to be embedded within the inner fibers and graphene sheets, which are beneficial to provide more defects and pores for adsorption. Without binder, such a tri-component carbon electrode has an electro sorption capacity as high as 13.6 mg g^{-1} in 500 mg L^{-1} NaCl aqueous solution. Therefore, the tri-component carbon electrode was demonstrated to meet CDI requirements for brackish and sea water desalination.

2. Experimental

2.1. CNT purification

MWCNTs (25 mg) in a mixture of concentrated sulphuric and nitric acids (3:1 volume ratio) were heated at reflux with for 3 h at 70°C. The mixture was diluted with an abundant amount of water in a water bath to ensure the temperature stayed below 70°C after cooling to room temperature. They were filtrated and then dried in the vacuum oven at 70°C overnight to obtain CNTs powders.

2.2. Preparation of RG/CNT/C nanofibers membrane

Polyacrylonitrile (PAN, M_w = 150000 g mol^{-1}, Aldrich, 99.8%) was dispersed in N, N-dimethylformamide (DMF, Sinopharm Chemical Reagent Co., Ltd, China) to prepare 10 wt.% PAN solution. Experimental details of GO preparation can be found in the Supplementary data. Then, the well-dispersed GO (10 wt.% vs. PAN)and CNTs in DMF were added into the PAN/DMF solution. The solution was kept at 60°C under continuous stirring for 8 h to yield a GO/CNT/PAN suspension.

The GO/CNT/PAN solution was put into a 10 mL syringe with a spinning steel needle. Then, electro spinning was undertaken at a flow rate of 1.0 mL h^{-1} and a high voltage of 19 kV. The electro spun fibers were collected on the grounded aluminum foil, 15 cm away the syringe needle. The fiber sheet collected was dried in a vacuum at 70°C for 8 hand stabilized at 280°C in air for 2 h with a heating rate of 1°C min^{-1}. Afterward, the fiber membrane was further heated to 800°C in a tube furnace for 2 h at a heating rate of 5°C min^{-1} under a continuously flowing N$_2$, and then, CO$_2$ was used to activate the nanofiber membrane for 1 h to obtain RG/CNT/C tri-component nanofiber electrodes. The weight ratio between PAN and GO was set at 10:1. The as-fabricated RG/CNT/C composite membrane with the CNT content varying at 5, 10, 15 wt.% vs GO. The prepared nanofiber samples were denoted as RG/CNT-X/C, where X stands for the weight percentage of CNTs in the nanofibers. For comparison, pristine CNF membrane and RG/C nanofiber membrane were also prepared in the same condition. The procedure for the carbon nanofiber preparation is illustrated in Fig. S1.

2.3. Characterization

The X-ray powder diffraction (XRD) measurements were performed on Bruker D8 Advance XRD instrument (Bruker, Cu Kα radiation). The SEM images of the samples were obtained using a high-resolution field-emission scanning electron microscope (Philips XL 30FEG, acceleration voltage of 30 kV). A transmission electron microscope (TEM, Hitachi H-800) was further used for characterization of the micro structure of the samples. The quality of carbon samples was identified by using a laser confocal Raman spectrometer (Nicolet NXR 9650 FT-Raman spectrometer, 632.8 nm). To measure the electrical resistance, the CNF and RG/CNT-10/C films were measured by the four-wire method (Keithley, 2000). Brunauer–Emmett–Teller (BET) surface area and pore structural properties were evaluated with N$_2$ adsorption at 77 K (Micro metrics, ASAP2460). The samples were degassed at 200°C for about 12 h before measurements. The cyclic voltammetry (CV) tests and electrochemical impedance spectroscopy (EIS) measurements were carried out on CHI 660D electrochemical workstation (Shanghai Chenhua Instruments) in 1.0 M NaCl solution with a three-electrode mode, including a saturated calomel electrode (SCE) as reference and platinum foil as the counter electrode. The specific capacitance (C, F g^{-1}) can be obtained from the CV curves according to the following equation [26]:

$$C = \frac{\int IdV}{mv\Delta V} \tag{1}$$

where I(A) is the response current density, ΔV (V) is the potential window, v (V s^{-1}) is the potential scan rate and m (g) is the mass of the electrode material.

2.4. Desalination test

NaCl concentration was obtained at room temperature according to a calibration curve of ion conductivity (µS cm⁻¹) and NaCl concentration (mg L⁻¹) made prior to the experiment (Fig. S2). Electro sorption experiments were conducted. A single CDI cell (Fig. S3) was prepared using the as-made electrodes (50 mm × 20 mm), as shown in Fig. 1. The electrodes attached to titanium mesh were used as the current collector which was connected to the power supply and the Nylon mesh (~1 mm) was used as a spacer in the assembly. The silicon gasket was used to seal the cell. During the electro sorption process, batch mode experiments were carried out in a continuously recycling system. The solution was continually pumped into the CDI cell with a constant rate of 25 mL min⁻¹, and the effluent was returned to the sell by the peristaltic pump. The volume of the solution was maintained at 50 ml. As the working voltage of 1.0–1.4 V was applied, the concentration change of NaCl solution was monitored on line at 25°C by a conductivity meter. The electro sorptive capacity (Q, mg g⁻¹) was calculated by the following equation [18]:

$$Q = \frac{(C_0 - C_t)V}{M} \tag{2}$$

where C_0 and C_t (mg L⁻¹) are the initial and final NaCl concentrations, V (L) is the total volume saline solution, and M (g) is the total mass of the electrodes.

The charge efficiency (Λ) is computed from the following equations [27,28]:

$$\Lambda = \frac{\Gamma \times F}{\Sigma} \tag{3}$$

where Γ is the electro sorption capacity (mol g⁻¹), F is the Faraday constant (96485 C mol⁻¹), and Σ is the total charge transferred between the electrode (C g⁻¹).

3. Results and discussion

3.1. Morphology and structure characterization

Fig. 1 shows the optical and FESEM images of RG/CNT-10/C nanofiber (NF)web. The carbonized RG/CNT-10/C shows a continuous monolithic surface with high structural flexibility. The SEM image shows a cross linked fibrous structure (Figs. 1b and S4). Fig. 1c shows that RG sheets distributed among CNFs. The CNFs had a diameter in the range of 150–250 nm. The magnified area in Fig. 1c indicated that the graphene nanosheets and CNTs were closely jointed
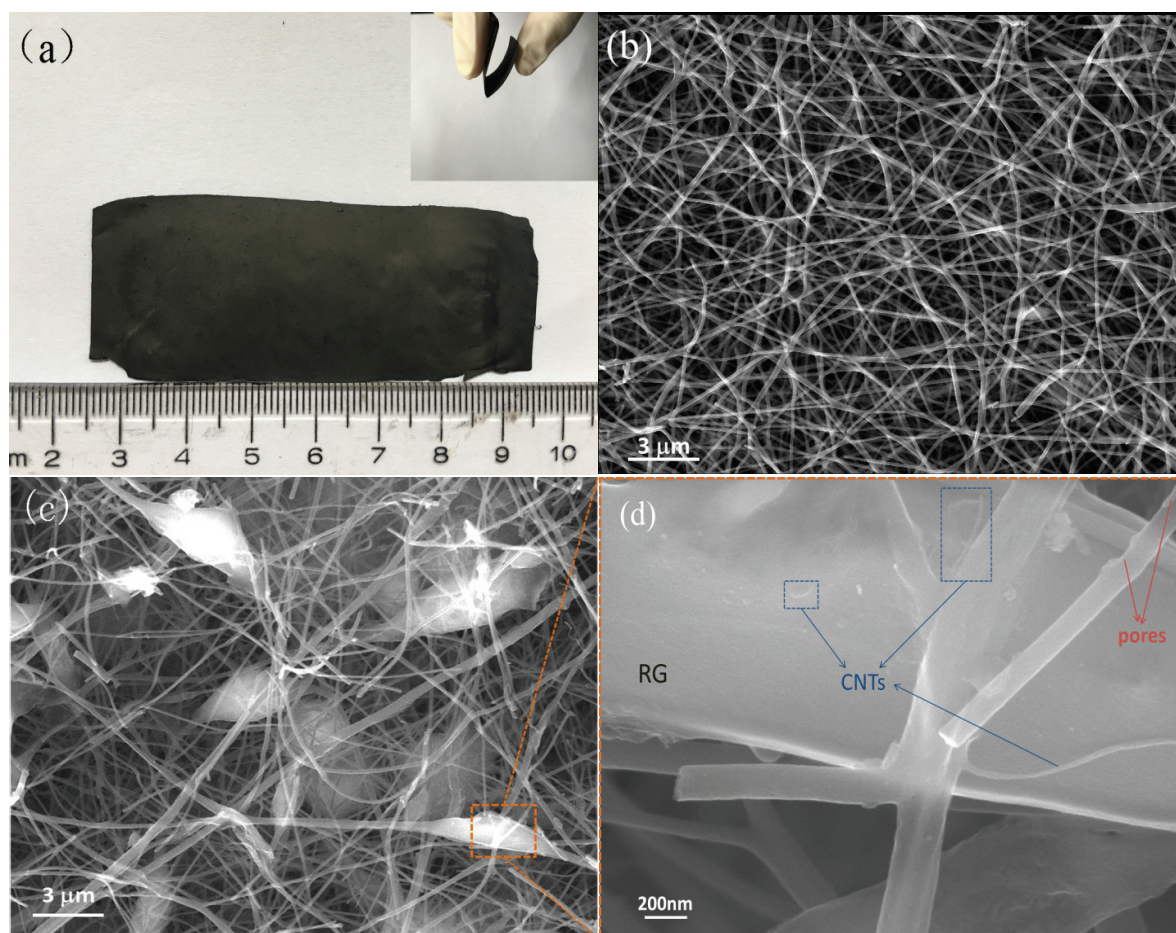

Fig. 1. (a) Optical image of RG/CNT-10/C, (b) SEM images of CNF, (c) Low- and (d) High-magnification SEM images of RG/CNT-10/C.

to the CNF segments to form a three-dimensional (3D) network structure (Fig. 1d). Due to the difference in thermal shrinkage between CNTs and CNF, novel defects and pores were formed on the surface of the fibers (Fig. S5).

TEM images shown in Fig. 2 provide more information about the internal of the RG/CNT-10/C. Fig. 2 show that the CNTs (a diameter of about 30 nm) and RG were firmly connected at the intersection parts of the carbon nanofibers. Moreover, some of CNTs were twined with RG sheet and fibers, and some of CNTs were embedded within the inner fibers. This novel structure not only facilitates to decrease the aggregation of CNT bundle, but also enhanced the transportation of electrons at the junction. Some defects and pores formed by the introduction of CNTs, which are beneficial to provide more adsorption sites for salt ions.

The electrical resistance of the CNF and RG/CNT-10/C samples was measured using a 4-probe method. RG/CNT-10/C has an average conductivity of 45.3 Sm^{-1}, which is higher than that of the CNF sample (3.6 Sm^{-1}). The higher conductivity indicates that RG/CNT-10/C has higher electron transfer efficiency, which is attributed to the presence of CNTs and RG in the structure.

The XRD patterns of as-made membranes are shown in Fig. 3a. For the RG, a single diffraction peak appeared at 26.2°, corresponding to the graphitic (002) face, which indicates successful exfoliation from graphitic [30]. The RG/CNT-10/C showed a peak at around $2\theta = 27.1°$. The peak shift to the right indicates the enlarged distance between graphite layers [13]. However, the peak (002) width was much shorter, indicating that the RG is loosely stacked in RG/CNT-10/C.

Fig. 3b shows Raman spectra of the CNFs, RG/CNFs, and RG/CNT-10/C NFs in the region of 800–2200 cm^{-1}. All of as-spun webs exhibit two prominent peaks at around 1350 (D-band) and 1600 (G-band) cm^{-1}. The intensity ratio of D band to G band (ID/IG) indicates graphitization degree [32]. For CNFs, RG/CNFs and RG/CNT-10/CNFs, the ID/IG values were 1.33, 1.28 and 1.12, respectively. This indicates that the tri-component nanofibers have higher degree of graphitic structure
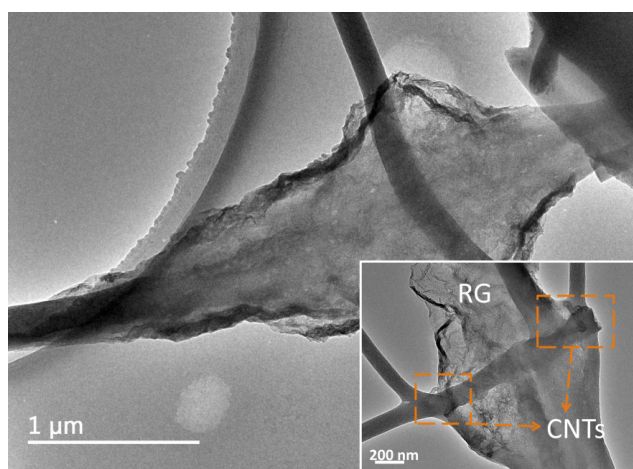
than CNFs. Moreover, the presence of RG and CNTs in the carbon nanofibers is beneficial for the charge transfer in the adsorption process. The N_2 adsorption/desorption isotherm in Fig. 3c depicts the RG/CNT-10/C NF, RG/C NF and CNF hysteresis loop, which is the type-IV

Fig. 2. TEM micro graphs of RG/CNT-10/C after carbonization at low and high (inserted picture) magnifications.
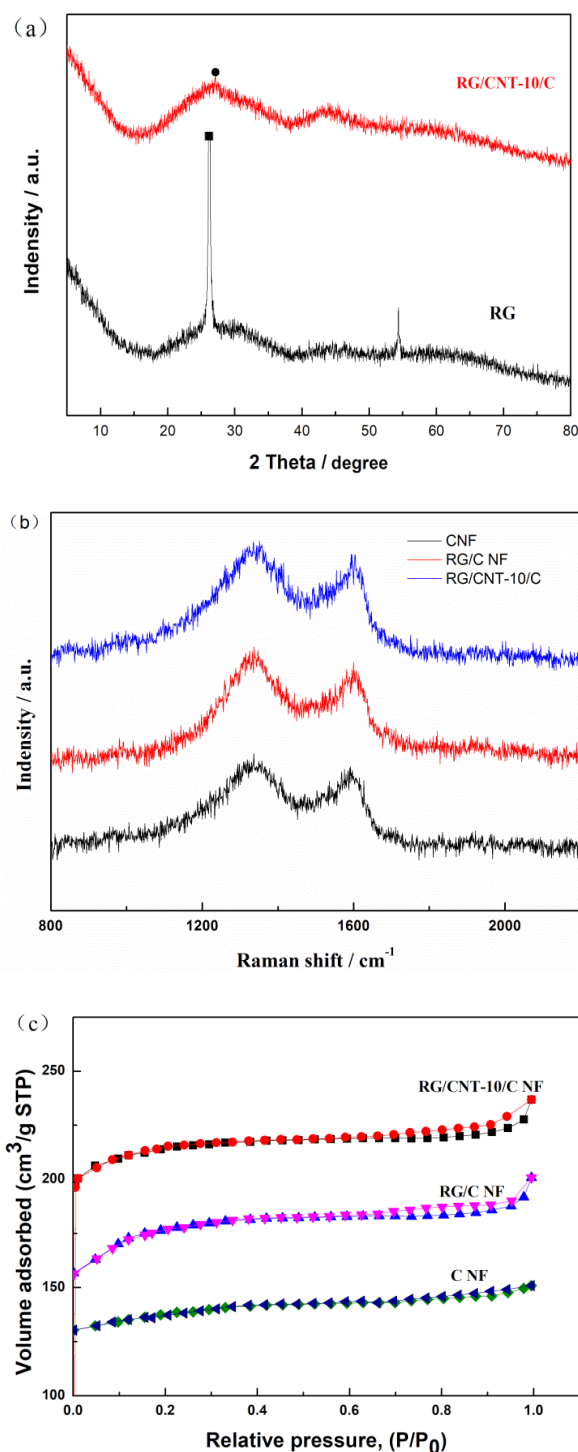

Fig. 3. (a) XRD patterns of RG and RG/CNT-10/C, (b) Raman spectra of CNF, RG/CNF, andRG/CNT-10/C, (c) N_2 adsorption-desorption isotherms at 77 K.

adsorption isotherm pattern with a hysteresis loop at a relative pressure $P/P_0 > 0.5$ [13,33]. It confirms that the mesoporous structure is present in synthesized RG/CNT-10/C samples. The specific surface area, mesopore volume and average pore size of the synthesized CNF and RG/CNT-10/C are summarized in Table 1. It can be seen that the specific surface area of RG/CNT-10/C is 634 $m^2 g^{-1}$. Moreover, the mesopore volume (0.143 $cm^3 g^{-1}$) of RG/CNT-10/C is much larger than that of CNF. The average pore width of RG/CNT-10/C(2.05 nm) is bigger than CNF (1.6 nm). Clearly, the as-synthesized RG/CNT-10/C NF displays a highly porous structure.

Table 1
Textural characteristics of CNF and RG/CNT-10/C material electrodes

Materials	V_{meso} (cm^3 g^{-1})	S_{BET} (m^2 g^{-1})	D_{av} (nm)
CNF	0.058	509	1.6
RG/CNT-10/C	0.143	634	2.05

3.2. Electrochemical characterization

Cyclic voltammetry (CV) analysis is a powerful tool to examine the electrochemical performance of electrode materials [30]. Fig. 4a shows the cyclic voltammetry (CV) curves of CNFs, RG/C NFs, RG/CNT-5/C NFs, RG/CNT-10/C NFs and RG/CNT-15/C NFs in a potential range of –1.2 to 0.2 V (scan rate 5 mV s^{-1}) in a three-electrode mode at room temperature. The RG/CNT-10/C showed a symmetrical rectangular shape with the CV area larger than that of CNFs, RG/C NFs, RG/CNT-5/C NFs and RG/CNT-15/C NFs. Fig. 4b shows the CV profiles of RG/CNT-10/C electrode at scan rates of 5–100 mV s^{-1}. All the curves had no obvious oxidation/reduction peaks, suggesting that the electrode has an excellent capacitive behavior at different scan rates [19]. Moreover, a symmetric rectangular shape is still seen at a high scan rate of 50 mV s^{-1}, indicating an excellent double-layer capacitive performance. The specific capacitance of the CNF, RG/C NF, and RG/CNT-10/C NF samples gradually decreases with the increase in scan rate (Fig. 4c). RG/CNT-10/C has a higher specific capacitance than CNFs and RG/C NFs, indicating that the RG/CNT-
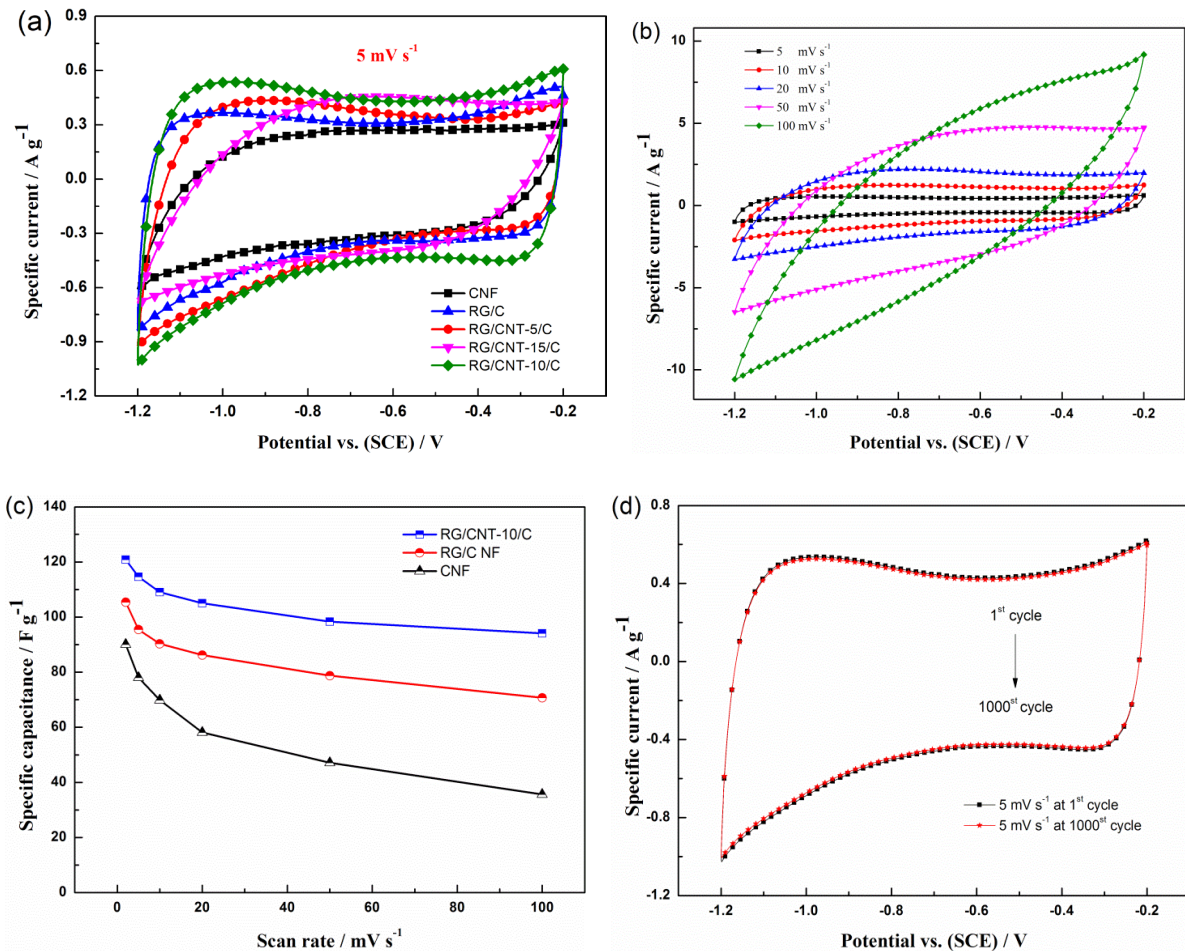

Fig. 4. (a) CV curves of CNF, RG/CNF, RG/CNT-5/C,RG/CNT-10/C and RG/CNT-15/C in 1 M NaCl solution at a sweep rate of 5 mV s^{-1}; (b) CV curves of RG/CNT-10/C at different scan rates in 1 M NaCl solution; (c) Comparison of the specific capacitance between CNF, RG/CNF, and RG/CNT-10/C electrode at different scan rates; (d) CV curves for RG/CNT-10/C composite at 5 mV s^{-1} scan rate before and after 1000 cycles.

10/C electrode can adsorb and desorb ions more quickly and efficiently than the other electrodes.

The specific capacitance was calculated according to Eq. (1). The calculated capacitance of RG/CNT-10/C electrode was much higher than that of the CNFs and RG/C NFs. Even at a high scan rate of 100 mV s⁻¹, the specific capacitance of CNF, RG/C NF and RG/CNT-10/C NF remains at 39.6%, 67.1% and 78.2%, respectively. Clearly, the addition of GO and CNTs in the electro spinning solution assist to improve the electrode electrochemical stability. After 1000 cycles of charging-discharging at the scan rate of 5 mV s⁻¹, the RG/CNT-10/C electrode still had 98% of capacitance retention (Fig. 4d).

Electrochemical impedance spectroscopy (EIS) was used to examine the electrical properties of CNF, RG/C NF, and RG/CNT-10/C NF electrodes. As shown in Fig. 5, the Nyquist plots of each sample show similar shapes, which comprised of a small quasi-semicircle in the high frequency region and a linear segment in the low frequency region. The high-frequency arc is derived from the double layer capacitance (C_{dl}) in parallel with the charge transfer resistance (R_{ct}) between the electrolyte and the electrodes [31,34]. The diameter of the semicircle for RG/CNT-10/C was smaller than that of RG/C NFs and CNFs, implying that the optimal ratio of CNT and RG will result in a much lower charge transfer resistance, and thus improve the capacitive performance.

3.3. Electro sorption performance

The CDI experiments were performed in a NaCl solution with an initial concentration of 100 mg L⁻¹. For comparison, RG/CNT-5/C, RG/CNT-10/C, and RG/CNT-15/C were tested in the same condition. Fig. 6a shows the electro sorption process reaches a maximum value after approximately 35 min. The inset in Fig. 6a is the corresponding electro sorption capacity of CNF, RG/C NF, and RG/CNT-X/C NF electrodes. The electro sorption capacity and charge effi-
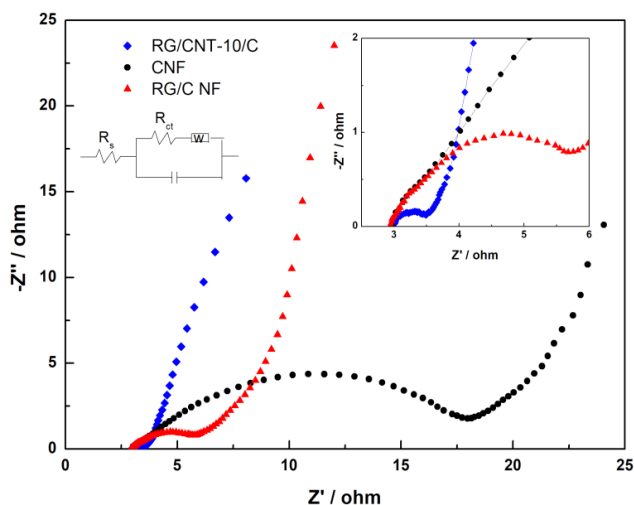
ciency of RG/CNT-10/C was calculated being 8.8 mg g⁻¹ and 0.78, which was much higher than those of RG/C NFs (6.9 mg g⁻¹ and 0.66) and the others [35].

Adsorption kinetics was used to gain better understanding of the CDI adsorption process. A pseudo-first-order adsorption model was employed to fit adsorption kinetics of RG/CNT-10/C and CNFs using the equation [34,36]:

$$\log\left(q_e - q_t\right) = \log q_e - \frac{kt}{2.703} \tag{4}$$

where k (min⁻¹) is the adsorption rate constants, q_e (mg g⁻¹) and q_t (mg g⁻¹) are the NaCl adsorption capacities at equilibrium and time t (min), respectively.

Fig. 6b shows the nonlinear fitting between the experimental data and Eq. (4). The coefficients of the kinetic equation are summarized in Table 2. The regression coefficient R²

Fig. 5. Nyquist plot (inset shows a close-up of near origin section of the figure) for three samples in the frequency range of 0.01 Hz-100 kHz.
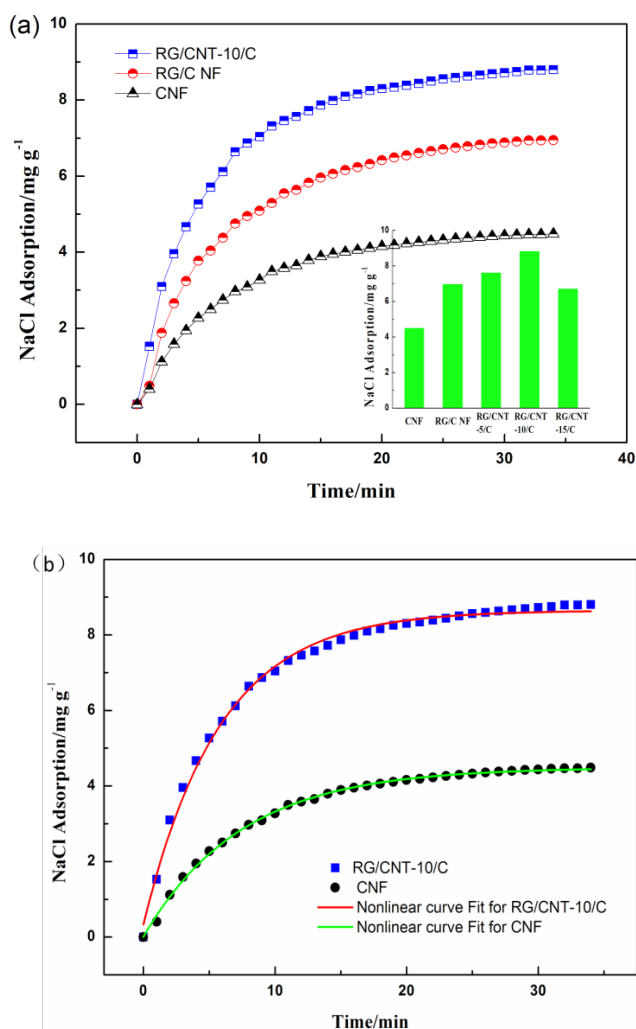

Fig. 6. (a) Variation of NaCl adsorption during electro sorption process for CNF, RG/CNF, and RG/CNT-10/C electrodes in NaCl solution with a feeding NaCl solution (100 mg L⁻¹) at an applied voltage of 1.2 V. Inset is the corresponding electro sorption capacity of CNF, RG/CNF, and RG/CNT-X/C electrodes; (b) Experimental data as well as the simulated line by adopting the pseudo-first-order adsorption equation for RG/CNT-10/C and CNF.

for RG/CNT-10/C and CNFs is 0.989 and 0.996 (very close to 1), which means that the adsorption equation is very suitable for the experimental data. Further, the rate constant for RG/CNT-10/C was higher than that for CNFs, indicating that the ions inside RG/CNT-10/C transport much faster than that in CNFs. We believe that the addition of RG and CNTs to CNFs significant enhances ion transport.

Fig. 7 shows the further investigation of the CDI performance from the effects of different applied voltages and

Table 2
Coefficients of kinetic equation for RG/CNT-10/C and CNFs

Materials	R^2	k
RG/CNT-10/C	0.989	0.468
CNF	0.996	0.362

(a)

(b)

concentrations of NaCl solution. As shown in Fig. 7a, the NaCl concentration decreases fast at the initial phase and then slows down to a steady state. As expected, the NaCl adsorption capacity increases significantly at a larger applied voltage. However, the applied voltage of 1.4 V is higher than the potential for the break-down of water, 1.24 V. Fig. 7b displays the NaCl adsorption capacity curves of RG/CNT/C NF electrode at different initial concentrations of NaCl solution. As can be seen in Fig. 7b, the electro sorption capacities are 8.8 mg g^{-1} (C_0 = 100 mg L^{-1}), 10.9 mg g^{-1} (C_0 = 300 mg L^{-1}), and 13.6 mg g^{-1} (C_0 = 500 mg L^{-1}). Obviously, the NaCl adsorption capacity increases with the increase of NaCl solution concentration. It can be seen that the charge efficiency Λ increases with the increase of the applied voltage or concentration, which is consistent to that reported in the literature [28].

To examine the cyclic operation and regeneration performance of RG/CNT/C NF electrode, continuous electro sorption–desorption experiment in NaCl solution with an initial conductivity of 200 μS cm^{-1} was carried out at an applied cell potential of 1.2 V, as shown in Fig. 8. A cycle from electro sorption to regeneration needs about 80 min. In addition, RG/CNT/C NF electrode can be regenerated very well with no detectable degradation after over 20 cycles, confirming promising CDI performance.

In addition, we compared the electro sorption capacity between our RG/CNT-10/C and the carbon electrode materials reported in the literatures (Table 3). Without binder, such a tri-component carbon electrode has an electro sorption capacity as high as 8.8 mg g^{-1} in 100 mg L^{-1} NaCl aqueous solution. The enhanced electro sorption capacity of the RG/CNT-10/C electrodes was proposed to come from the following reasons: (1) the mesopore structure formed by the introduction of CNTs could provide more sites to accommodate the ions; (2) RG/CNT-10/C electrode exhibits lower electrical resistance than RG/CNF, indicating that a high-efficiency electron transfer; (3) the 3D porous network structure composed of RG and CNTs jointed to the CNF segments without binders can provide a better synergistic effect.
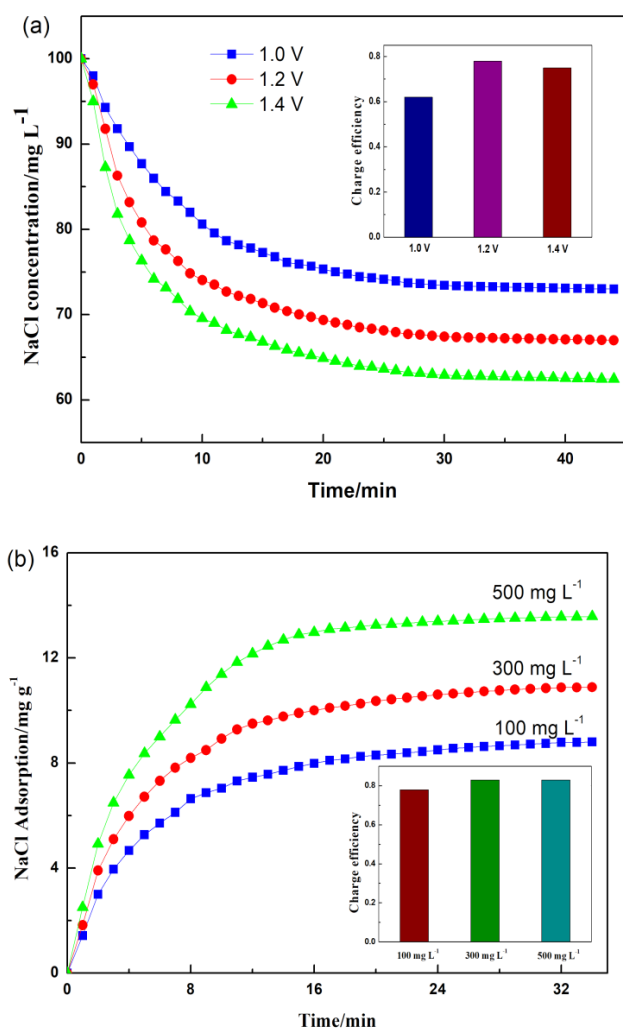

Fig. 7. CDI performance of the RG/CNT-10/C electrode: (a) the variation of NaCl concentration along with time in a 100 mg L^{-1} NaCl solution at different applied voltage. Inset in (a) shows corresponding charge efficiency; (b) the adsorption curves in different concentrations of NaCl solution at a voltage of 1.2 V. Inset in (b) shows corresponding charge efficiency.
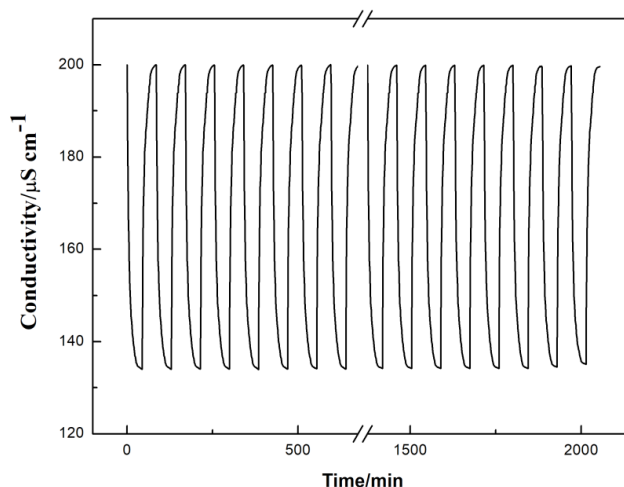
Fig. 8. Recycle electro sorption experiment for RG/CNT-10/C electrode.

Table 3
Comparison of electro sorption capacity and charge efficiencies of various carbon electrodes

Materials	Year	Initial concentration (mg L^{-1})	Cell potential (V)	Electro sorption capacity (mg g^{-1})	Charge efficiency	Ref.
AC	2010	200	1.5	3.7	0.43	[37]
CNF	2012	81	1.6	4.6	–	[38]
CNT/CNF	2015	400	1.2	6.4	0.25	[39]
rGO/CNF	2014	400	1.2	7.2	–	[13]
CB/CNF	2012	90	1.6	9.13	–	[29]
DMSO$_2$/PCNF	2015	500	1.2	8.1	0.58	[25]
S-RGO/ACF	2016	100	1.2	9.2	0.85	[40]
bcCNF800	2015	200	1.2	6.72	0.69	[28]
PCNF	2016	100	1.2	6.51	0.33	[41]
RG/CNT/C	–	100	1.2	8.8	0.78	Present work

4. Conclusions

We have proved a facile method to prepare a tri-component binder free carbon sheets by electro spinning of PAN precursor containing GO and CNTs and subsequent carbonization. The as-fabricated carbon nanofiber sheets can be used directly as CDI electrodes. We have successfully enhanced electron transfer due to the 3D network structure formed by the introduction of CNTs and thermal activation. Moreover, in a 500 mg L^{-1} NaCl solution, the electrodes showed a desalination capacity of 13.6 mg g^{-1} at 1.2 V, which is higher than those of CNFs without GO and CNTs. The present study proves the important role of the introduction of GO and CNTs in the fabrication of mesopores and ion removal. It provides a basis for the choice of deionization electrode materials and CDI application potentials.

Acknowledgments

References

[1] T. Humplik, J. Lee, S.C. O'hern, B.A. Fellman, M.A. Baig, S.F. Hassan, M.A. Atieh, F. Rahman, T. Laoui, R. Karnik, E.N. Wang, Nanostructured materials for water desalination, Nanotechnology, 22 (2011) 292001.
[2] F.A. Al Marzooqi, A.A. Al Ghaferi, I. Saadat, N. Hilal, Application of capacitive deionisation in water desalination: a review, Desalination, 342 (2014) 3–15.
[3] M.A. Anderson, A.L. Cudero, J. Palma, Capacitive deionization as an electrochemical means of saving energy and delivering clean water. Comparison to present desalination practices: Will it compete? Electro chim. Acta, 55 (2010) 3845–3856.
[4] C. Feng, C.C. Tsai, C.Y. Ma, C.P. Yu, C.H. Hou, Integrating cost-effective microbial fuel cells and energy-efficient capacitive deionization for advanced domestic wastewater treatment, Chem. Eng. J., 330 (2017) 1–10.
[5] M.E. Suss, V. Presser, Water desalination with energy storage electrode materials, Joule, 2 (2018) 10–15.
[6] C. Zhao, G. Liu, N. Sun, X. Zhang, G. Wang, Y. Zhang, H. Zhang, H. Zhao, Biomass-derived N-doped porous carbon as electrode materials for Zn-air battery powered capacitive deionization, Chem. Eng. J., 334 (2018) 1270–1280.
[7] M. Andelman, Non-fouling flow through capacitor system, US Pat., (1998) 5779891-A.
[8] L. Pan, X. Wang, Y. Gao, Y. Zhang, Y. Chen, Z. Sun, Electro sorption of anions with carbon nanotube and nanofibre composite film electrodes, Desalination, 244 (2009)139–143.
[9] L. Liu, G. Qiu, S.L. Suib, F. Liu, L. Zheng, W. Tan, L. Qin, Enhancement of Zn^{2+} and Ni^{2+} removal performance using a deionization pseudo capacitor with nanostructured birnessite and its carbon nanotube composite electrodes, Chem. Eng. J., 328 (2017) 464–473.
[10] C.J. Yan, L.D. Zou, R. Short, Polyaniline-modified activated carbon electrodes for capacitive deionization, Desalination, 333 (2014) 101–106.
[11] M. Zafra, P. Lavela, G. Rasines, C. Macias, J. Tirado, C. Ania, A novel method for metal oxide deposition on carbon aerogels with potential application in capacitive deionization of saline water, Electrochim. Acta, 135 (2014) 208–216.
[12] P. Xu, J.E. Drewes, D. Heil, G. Wang, Treatment of brackish produced water using carbon aerogel-based capacitive deionization technology, Water Res., 42 (2008) 2605–2617.
[13] Q. Dong, G. Wang, B. Qian, C. Hu, Y. Wang, J.Qiu, Electro spun composites made of reduced graphene oxide and activated carbon nanofibers for capacitive deionization, Electrochim. Acta, 137 (2014) 388–394.
[14] C. Yan, L. Zou, R. Short, Single-walled carbon nanotubes and polyaniline composites for capacitive deionization, Desalination, 290 (2012) 125–129.
[15] G. Luo, H. Li, D. Zhang, L. Gao, T. Lin, A template-free synthesis via alkaline route for Nb$_2$O$_5$/carbon nanotubes composite as pseudo-capacitor material with high-rate performance, Electro Chim. Acta, 235 (2017) 175–181.
[16] H. Wang, L. Shi, T. Yan, J. Zhang, Q. Zhong, D. Zhang, Design of graphene-coated hollow mesoporous carbon spheres as high performance electrodes for capacitive deionization, J. Mater. Chem. A., 2 (2014) 4739.
[17] C. Yan, Y.W. Kanaththage, R. Short, C.T. Gibson, L. Zou, Graphene/Polyaniline nanocomposite as electrode material for membrane capacitive deionization, Desalination, 344 (2014) 274–279.
[18] X. Chen, Y. Chen, A. Kumar, A. Mahmoud, J.A. Nychka, H.J. Chung, Sponge-templated macroporous graphene network for piezoelectric ZnO nanogenerator, ACS Appl. Mater. Inter., 7 (2015) 20753–20760.
[19] G.X. Li, P.X. Hou, S.Y. Zhao, C. Liu, H.M. Cheng, A flexible cotton-derived carbon sponge for high-performance capacitive deionization, Carbon, 101 (2016) 1–8.

[20] X. Xu, Z. Sun, D.H.C. Chua, L. Pan, Novel nitrogen doped graphene sponge with ultrahigh capacitive deionization performance, Sci. Rep., 5 (2015) 11225.

[21] Z.Y. Yang, L.J. Jin, G.Q. Lu, Q.Q. Xiao, Y.X. Zhang, L. Jing, X.X. Zhang, Y.M. Yan, K.N. Sun, Sponge-templated preparation of high surface area graphene with ultrahigh capacitive deionization performance, Adv. Funct. Mater., 24 (2014) 3917–3925.

[22] Z. Tai, X. Yan, J. Lang, Q. Xue, Enhancement of capacitance performance of flexible carbon nanofiber paper by adding graphene nanosheets, J. Power Sources, 199 (2012) 373–378.

[23] G. Luo, Y. Wang, L. Gao, D. Zhang, T. Lin, Graphene bonded carbon nanofiber aerogels with high capacitive deionization capability, Electrochim. Acta, 260 (2018) 656–663.

[24] J. Liu, S. Wang, J. Yang, J. Liao, M. Lu, H. Pan, L. An, ZnCl$_2$ activated electro spun carbon nanofiber for capacitive desalination, Desalination, 344 (2014) 446–453.

[25] H. Pan, J. Yang, S. Wang, Z. Xiong, W. Cai, J. Liu, Facile fabrication of porous carbon nanofibers by electro spun PAN/dimethyl sulfone for capacitive deionization, J. Mater. Chem. A., 3 (2015) 13827–13834.

[26] F. Lai, Y. Huang, L. Zuo, H. Gu, Y. E. Miao, T. Liu, Electro spun nanofiber-supported carbon aerogel as a versatile platform toward asymmetric super capacitors, J. Mater. Chem. A., 4 (2016) 15861–15869.

[27] S. Porada, L. Weinstein, R. Dash, A. Van Der Wal, M. Bryjak, Y. Gogotsi, P.M. Biesheuvel, Water desalination using capacitive deionization with micro porous carbon electrodes, ACS Appl. Mater. Inter., 4 (2012) 1194–1199.

[28] Y. Liu, T. Lu, Z. Sun, D.H.C. Chua, L. Pan, Ultra-thin carbon nanofiber networks derived from bacterial cellulose for capacitive deionization, J. Mater. Chem. A., 3 (2015) 8693–8700.

[29] G. Wang, Q. Dong, Z. Ling, C. Pan, C. Yu, J. Qiu, Hierarchical activated carbon nanofiber webs with tuned structure fabricated by electro spinning for capacitive deionization, J. Mater. Chem., 22 (2012) 21819–21823.

[30] D. Zhang, T. Yan, L. Shi, Z. Peng, X. Wen, J. Zhang, Enhanced capacitive deionization performance of graphene/carbon nanotube composites, J. Mater. Chem., 22 (2012) 14696–14704.

[31] Z. Peng, D. Zhang, T. Yan, J. Zhang, L. Shi, Three-dimensional micro/mesoporous carbon composites with carbon nanotube networks for capacitive deionization, Appl. Surf. Sci., 282 (2013) 965–973.

[32] J.G. Wang, Y. Yang, Z.H. Huang, F. Kang, Synthesis and electrochemical performance of MnO$_2$/CNTs–embedded carbon nanofibers nanocomposites for super capacitors, Electro chim. Acta, 75 (2012) 213–219.

[33] A.G. El-Deen, R.M. Boom, H.Y. Kim, H. Duan, M.B. Chan-Park, J.H. Choi, Flexible 3D nanoporous graphene for desalination and bio-decontamination of brackish water via asymmetric capacitive deionization, ACS Appl. Mater. Inter., 8 (2016) 25313–25325.

[34] H. Li, S. Liang, J. Li, L. He, The capacitive deionization behaviour of a carbon nanotube and reduced graphene oxide composite, J. Mater. Chem. A., 1 (2013) 6335–6341.

[35] M.E. Suss, S. Porada, X. Sun, P.M. Biesheuvel, J. Yoon, V. Presser, Water desalination via capacitive deionization: what is it and what can we expect from it? Energ. Environ. Sci., 8 (2015) 2296–2319.

[36] A.E. Rodrigues, C.M. Silva, What's wrong with Lager green pseudo first order model for adsorption kinetics? Chem. Eng. J., 306 (2016) 1138–1142.

[37] Y.J. Kim, J.H. Choi, Enhanced desalination efficiency in capacitive deionization with an ion-selective membrane, Sep. Purif. Technol., 71 (2010) 70–75.

[38] G. Wang, C. Pan, L. Wang, Q. Dong, C. Yu, Z. Zhao, J. Qiu, Activated carbon nanofiber webs made by electro spinning for capacitive deionization, Electro chim. Acta, 69 (2012) 65–70.

[39] Q. Dong, G. Wang, T. Wu, S. Peng, J. Qiu, Enhancing capacitive deionization performance of electro spun activated carbon nanofibers by coupling with carbon nanotubes, J. Colloid Interface Sci., 446 (2015) 387–392.

[40] G. Wang, Q. Dong, T. Wu, F. Zhan, M. Zhou, J. Qiu. Ultra sound-assisted preparation of electro spun carbon fiber/graphene electrodes for capacitive deionization: Importance and unique role of electrical conductivity, Carbon, 103 (2016) 311–317.

[41] G. Wang, B. Qian, Y. Wang, Q. Dong, F. Zhan, J. Qiu, Electro spun porous hierarchical carbon nanofibers with tailored structures for super capacitors and capacitive deionization, New J. Chem., 40 (2016) 3786–3792.

Supplementary

GO preparation

3 g graphite powder, 3 g P_2O_5 and 3 g $K_2S_2O_8$ were added into 250 mL three necked flask, respectively, and then 50 ml of sulphuric acid was added to the powders and stirred at 80°C for 5 h. As the mixture cooled to room temperature, it was slowly diluted with deionised (DI) water. The pre-oxidized graphite powders were collected by filtration and then subjected to oxidation by a modified Hummers' method described as follows[1,2]. Firstly, 50 ml sulphuric acid was added to the powders in the three necked flask. After that, 15 g $KMnO_4$ powder was added gradually in an ice batches during stirring. When the mixture became dark-green, and then warmed it to 35°C with stirring for 2 h. After diluting with DI water, in the case of vigorous mechanical stirring, 20 mL of 30% H_2O_2 was added drop wise. The color of the mixture turned to golden yellow and bubbled. Finally, the supernatant was removed and washed with aqueous HCl solution and DI water by centrifugation and then the freeze-drying method was performed to dry GO samples as brown fluffy solid.
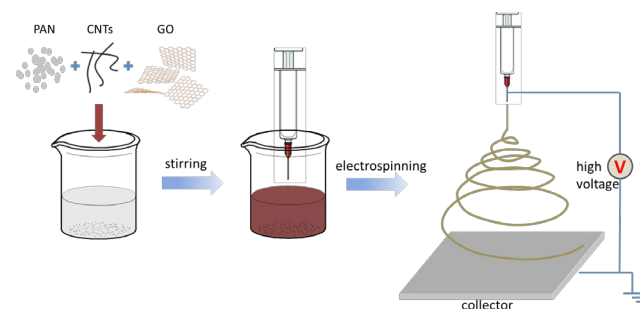

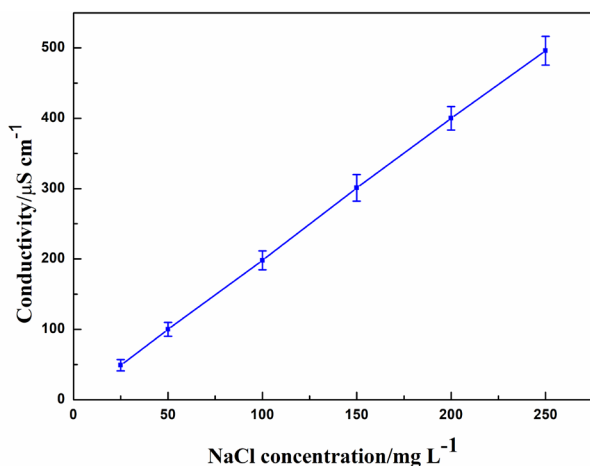Fig. S1. Schematic illustration for the fabrication of the RG/CNT/C tri-component composite membrane.

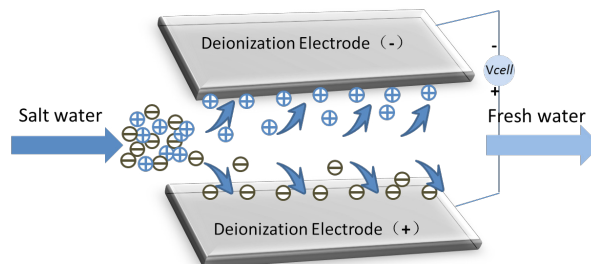Fig. S2. The calibration curve of ion conductivity and NaCl concentration.
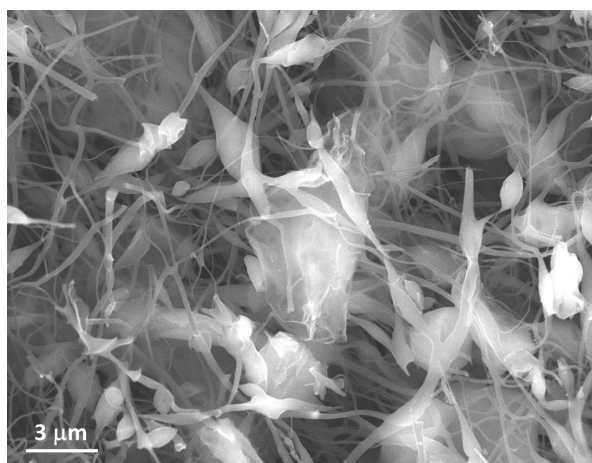

Fig. S3. Schematic diagram of a single CDI.
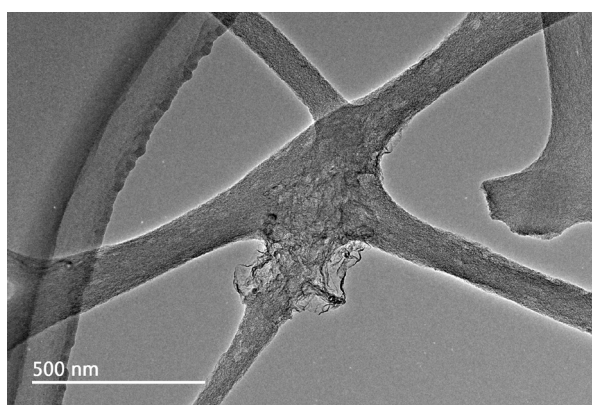

Fig. S4. SEM images of RG/C NF.

Fig. S5. TEM images of RG/CNT-10/C.

References

[1]   Y. Wimalasiri, L. Zou, Carbon nanotube/graphene composite for enhanced capacitive deionization performance, Carbon, 59 (2013) 464–471.
[2]   W.S. Hummers, R.E. Offeman, Preparation of graphitic oxide, J. Am. Chem. Soc., 80 (1958) 1339.